chemosensors

MDPI

Article

An Enzymatic Multiplexed Impedimetric Sensor Based on α-MnO_2/GQD Nano-Composite for the Detection of Diabetes and Diabetic Foot Ulcer Using Micro-Fluidic Platform

Ashish Mathur [1,2], Hari Chandra Nayak [3], Shailendra Rajput [4,*], Souradeep Roy [1], Shalini Nagabooshanam [5], Shikha Wadhwa [6] and Ranjit Kumar [6]

1 Centre for Interdisciplinary Research and Innovation (CIDRI), University of Petroleum and Energy Studies, Dehradun 248007, India; nanoashish@gmail.com (A.M.); souradeep.roy@ddn.upes.ac.in (S.R.)
2 Department of Physics, University of Petroleum and Energy Studies, Dehradun 248007, India
3 Department of Physics, Maharaja Chhatrasal Bundelkhand University, Chhatarpur 471001, India; drhc.nayak@mp.gov.in
4 Department of Electrical and Electronic Engineering, Ariel University, Ariel 40700, Israel
5 Department of Engineering Design, Indian Institute of Technology Madras, Chennai 600036, India; 011322@imail.iitm.ac.in
6 Department of Chemistry, University of Petroleum and Energy Studies, Dehradun 248007, India; shik.wadhwa@gmail.com (S.W.); ranjit.kumar@ddn.upes.ac.in (R.K.)
* Correspondence: shailendrara@ariel.ac.il

check for updates

Citation: Mathur, A.; Nayak, H.C.; Rajput, S.; Roy, S.; Nagabooshanam, S.; Wadhwa, S.; Kumar, R. An Enzymatic Multiplexed Impedimetric Sensor Based on α-MnO_2/GQD Nano-Composite for the Detection of Diabetes and Diabetic Foot Ulcer Using Micro-Fluidic Platform. *Chemosensors* **2021**, *9*, 339. https://doi.org/10.3390/chemosensors9120339

Academic Editors: Ilaria Rea, Luca De Stefano, Rosalba Moretta and Bruno Miranda

Received: 23 October 2021
Accepted: 30 November 2021
Published: 2 December 2021

Abstract: Diabetes is widely considered as a silent killer which affects the internal organs and ultimately has drastic impacts on our day-to-day activities. One of the fatal outcomes of diabetes is diabetic foot ulcer (DFU); which, when becomes chronic, may lead to amputation. The incorporation of nanotechnology in developing bio-sensors enables the detection of desired biomarkers, which in our study are glucose and L-tyrosine; which gets elevated in patients suffering from diabetes and DFUs, respectively. Herein, we report the development of an enzymatic impedimetric sensor for the multi-detection of these biomarkers using an electrochemical paper-based analytical device (μ-EPADs). The structure consists of two working electrodes and a counter electrode. One working electrode is modified with α-MnO_2-GQD/tyrosinase hybrid to aid L-tyrosine detection, while the other electrode is coated with α-MnO_2-GQD/glucose oxidase hybrid for glucose monitoring. Electrochemical impedance spectroscopy has been employed for the quantification of glucose and L-tyrosine, within a concentration range of 50–800 mg/dL and 1–500 μmol/L, respectively, using a sample volume of approximately 200 μL. The impedance response exhibited a linear relationship over the analyte concentration range with detection limits of ~58 mg/dL and ~0.3 μmol/L for glucose and tyrosine respectively, with shelf life ~1 month. The sensing strategy was also translated to Arduino-based device applications by interfacing the μ-EPADs with miniaturized electronics.

Keywords: diabetes; diabetic foot ulcer; α-MnO_2/GQD nano-composite; μ-EPADs; multiplexed monitoring; point-of-care

1. Introduction

The widespread outburst of diabetes has become a major concern, which is often termed as a silent killer, while also being considered the seventh alarming factor leading to an increased mortality rate. The worldwide prevalence has been estimated at 9% and is expected to rise to 10.4% by 2040 [1]. As per estimates, 7% of the population in India suffers from diabetes with the daily management of the condition and its complications placing a severe burden on healthcare resources [2]. One of the life-threatening consequences of diabetes is the occurrence of diabetic foot ulcers (DFUs). DFUs may be defined as the inflammation and infection of deep tissues which are associated with neurological abnormalities and various degrees of vascular disease in the lower limbs of humans [3].

The occurrence of DFUs is attributed to the application of high pressure, due to daily activities, in the feet of people suffering from diabetic peripheral neuropathy (DPN) [4–6], while several studies have also reported that low activity in patients suffering from DPN leads to DFU [7–9]. They are the major reasons for hospitalization since 34% of diabetics develop DFUs whereby another 50% need to undergo amputation(s), thereby impacting mobility and day-to-day activities which have placed a severe burden on already stretched resources [10,11]. While monitoring of diabetes has primarily been accomplished using the key biomarker—glucose, the conventional procedures for monitoring DFUs include Semmes-Weinstein monofilament, 128 Hz tuning fork, color Doppler, MRI, and temperature based methods [12]. However, these protocols cannot predict the occurrence of DFUs during its onset due to which the wound is allowed to become chronic and comorbid. A few more major disadvantages of these techniques include higher cost and time consumption. Search and discovery of differentially expressed indicators, such as biomarkers, has become imperative for the early monitoring of many diseases [13]. This also stands for DFU-specific biomarkers for its early monitoring.

Among various metabolites available in the wound fluid, the concentration of L-tyrosine becomes elevated from 67 to 311 μM [14]. Therefore, early and rapid monitoring of tyrosine quantities can effectively predict the occurrence of foot ulcers (DFUs) during their onset. The conventional implementation of high-performance liquid chromatography, chromatography–mass spectrometry, and capillary electrophoresis [15–17] suffer from issues, such as high cost, slow response, and expensive reagents, which currently limit their use. However, the extremely high prevalence of diabetes and resulting probability of occurrence of DFUs urges us to move towards developing a multiplexed platform whereby the patients will have options to monitor diabetes as well as predict the onset of foot ulcers. Such a miniaturized biosensor, when commercialized, would not only enable multiparametric monitoring but also ensure faster patient-doctor interactions so that timely diagnosis and treatment can be availed. This is possible by the incorporation of nanostructured materials as surface modifiers in electrochemical biosensors, the latter being highly efficient and sensitive as compared to optical and mass-based transducers.

Electrochemical nanobiosensing has been widely employed due to its simplicity, the potential for miniaturization, and rapid and stable response within a wide analyte concentration range [18–21]. Such features are primarily owed to the high surface area and quantum confinement effects of nanomaterials, which help in enhanced receptor immobilization and heterogeneous charge transfer that can potentially improve the overall device sensitivity and accuracy. Therefore, such bio-nanohybrid surfaces can be easily integrated onto flexible electrode platforms which have received huge attention in PoC-based healthcare monitoring [22]. Furthermore, IDTechEx have projected the market price of printed and flexible electrochemical sensors to reach an outstanding $8 billion mark by 2025 [23]. Such sensing platforms offer advantages, such as high stretchability, extremely lightweight, low cost, portability, easy disposability, and provisions of integration with miniaturized electronics for real-time data analytics [23].

Of various nanomaterials, the composite of α-MnO_2/graphene quantum dots (GQDs) has garnered much focus owing to the excellent catalytic and semiconducting properties of MnO_2 octahedral molecular sieves, along with exotic properties of GQDs. Few studies have focused on the application of MnO_2/GQDs in supercapacitors [24] and the development of fluorescence-based nanosensors for glutathione detection [25]. Meanwhile, the application of this nanocomposite towards developing a multiplexed sensing device has not yet been explored.

It is envisaged that the high surface area (and conductivity) of α-MnO_2 and GQDs, with the presence of native carboxyl groups in the latter, would enable the immobilization of glucose oxidase (GOx) and tyrosinase enzymes; which can lead to selective electrocatalysis for the detection of glucose and tyrosine, by enabling faster heterogeneous electron transfer due to quantum confinement effects. We believe that developing a portable device capable of monitoring diabetes and DFUs, as a function of glucose and tyrosine, is enormously

essential in identifying high-risk diabetics so that timely diagnosis and treatment can be availed for positive outcomes; since such a device is not yet available in the market.

2. Materials and Methods

2.1. Chemicals and Reagents

All the chemicals used in our research were of analytical grade and did not require further purification. L-tyrosine, citric acid, and sodium hydroxide (NaOH) were obtained from Sisco Research Laboratories Pvt Ltd., Mumbai, Maharashtra, India. Sodium di-hydrogen orthophosphate, di-sodium hydrogen orthophosphate, potassium ferrocyanide, and potassium ferricyanide were obtained from Fisher Scientific Pvt Ltd., Gujarat, India. Sodium chloride, potassium permanganate ($KMnO_4$), nitric acid, manganese chloride ($MnCl_2$), and isopropyl alcohol (IPA) were obtained from Merck Life Science Pvt Ltd., Karnataka, Bengaluru, India while tyrosinase, glucose oxidase, and D-glucose were purchased from Sigma Aldrich, St. Louis, MO, USA. Carbon conducting ink (resistivity ~50 kΩ cm) and 210 GSM (gram per square meter) A3 sheets were purchased from Nanoshell Pvt. Ltd., Wasatch Front, UT, USA and IndiaMART InterMESH Pvt. Ltd., Noida, India, respectively. All experiments were conducted in de-ionized (DI) water of ~18.2 MΩ cm resistivity.

2.2. Synthesis of Graphene Quantum Dots (GQDs)

GQDs were synthesized as per the protocol reported by Dong et al. [26]. Citric acid (2 gm) was suspended in 25 mL DI water and was heated to 200 °C. The liquified solution was observed to undergo a transition from colorless to pale yellow after 5 min, eventually turning orange after 30 min which confirmed the synthesis of GQDs. The resulting solution was carefully added to 10 mg/mL of NaOH while ensuring vigorous stirring. The pH was eventually adjusted to pH 7.0 in order to yield an aqueous solution of GQD.

2.3. Synthesis of α-MnO_2/GQD Nanocomposite

Initially, $MnCl_2$ aqueous solution was made by adding ~6 g of the compound in 17 mL double distilled water (DDW) (solution A). For solution B, 3.475 g $KMnO_4$ was added in 56 mL DDW followed by 1.7 mL concentrated HNO_3. This process essentially ensures the synthesis of α-MnO_2 as reported by Dubey et al. and Kumar et al. [27,28]. The next step involves the addition of GQD solution (5 mL) into solution A under 20 min of ultrasonication, followed by dropwise addition of solution B into solution A under stirring conditions. The mixture thus obtained was refluxed for 16 h at 100 °C, yielding a dark brownish precipitate. The latter was filtered and thoroughly washed with DDW (double distilled water) in order to obtain pH 7.0. The resulting sample (α-MnO_2/GQD) was left for drying at 120 °C for 12 h, and finally calcined at 300 °C for 6 h.

2.4. Characterization of α-MnO_2/GQD Nanocomposites

The morphological analysis was performed using a Zeiss EVO18 scanning electron microscope for powdered samples at a voltage of 10 kV interfaced with an EDX (energy dispersive X-ray) module. Further clarity on the morphology of the nanocomposite was achieved from transmission electron microscopy (TEM), which was performed at a beam energy of 120 keV. On the other hand, molecular fingerprint and functional group identification were analyzed using Fourier transform infrared spectroscopy (FTIR) within 4000–500 cm^{-1}. The spectrum was recorded by Perkin Elmer FTIR L125000P interferometer.

2.5. Sensor Fabrication

The paper-based electrodes were fabricated by printing using a silk screen consisting of a laser-patterned solid film comprised of the electrode designs [20]. The resulting screen was then placed on top of the 210 GSM (gram per square meter) A3 cellulose sheets having dimensions 3 cm × 1.5 cm × 0.5 mm (approx.), and carbon conducting ink was pressed using a squeegee, eventually generating the two working (diameter ~1 mm each) and one counter electrode patterns. The resulting multiplexed sensing strip is shown in Figure 1

below, where the subsequent steps for sensor fabrication are highlighted. The conducting ink-printed paper electrodes were allowed to dry at room temperature for 1 h before employing in electroanalytical sensing of glucose and tyrosine.

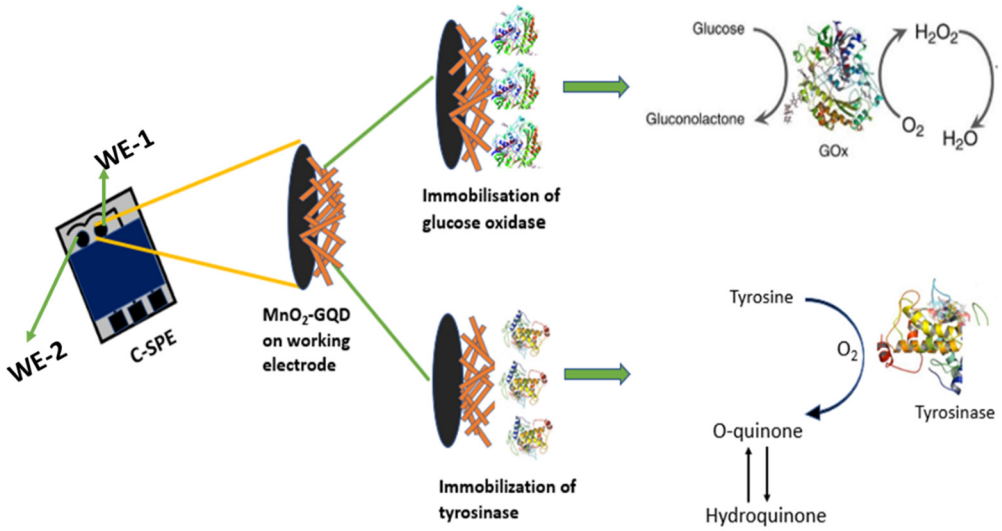

Figure 1. Steps involved in the fabrication of microfluidic multiplexed paper-based sensing strip.

The working electrodes (~1 mm diameter) were initially modified with 2 µL α-MnO_2/GQD, the latter being prepared as a suspension of 30% in IPA. After allowing the working electrodes to dry at room temperature for 30 min, 2 µL of GOx and tyrosinase enzymes were immobilized onto the nano-modified working electrodes (WE-1 and WE-2, respectively), for selective electro-catalysis of glucose and tyrosine, respectively (Figure 1). Specifically, GOx oxidizes glucose to gluconolactone while tyrosinase catalyzes tyrosine by initiating a redox cycling between O-quinone and hydroquinone. The sensing strips were then stored at 4 °C for 24 h followed by implementation in electrochemical sensing analysis.

3. Results

3.1. Surface Characterization of α-MnO_2/GQD Nanocomposites

The morphology analysis in Figure 2a reveals uniformly distributed nanostructures of α-MnO_2 possessing nanofibrous features. The average length and diameter of α-MnO_2 nanofibers were ~1 µm and ~45 nm, respectively, which are consistent with earlier reports [29].

Meanwhile, the presence of Mn and C, corresponding to α-MnO_2 and GQD, respectively, is confirmed from EDX mapping shown in Figure 2b, which is the first indication of nanocomposite formation. The TEM micrograph of Figure 2c, which has been captured on a single nanofiber, indicates layered structures of the α-MnO_2/GQD nanocomposite. It is possible to confirm that the presence of graphitic structure is attributed to the formation of several thick layers arranged in stacks. Furthermore, the oxidation of graphite layers resulted in morphology variations, as observed by the presence of wrinkled appearance with several folds. It can be observed that this product consists of nanosphere/nanofiber hierarchical nanostructures with an average nanodot diameter of ~10 nm. The FTIR spectrum of α-MnO_2/GQD nanostructures, as shown in Figure 2d, demonstrated a broad envelope between 3400 and 3000 cm^{-1}, corresponding to OH stretching vibrations. The doublet around 500 cm^{-1} and a singlet peak at 718 cm^{-1} can be attributed to the Mn-O bending modes of octahedral MnO_6 structures [30]. While the presence of GQDs in the fiber matrix was confirmed by the C=C and C-O bending vibrations in the graphitic plane at 1580 cm^{-1} and 1377 cm^{-1}, respectively [31], thereby confirming the formation of MnO_2/GQD nanocomposites.

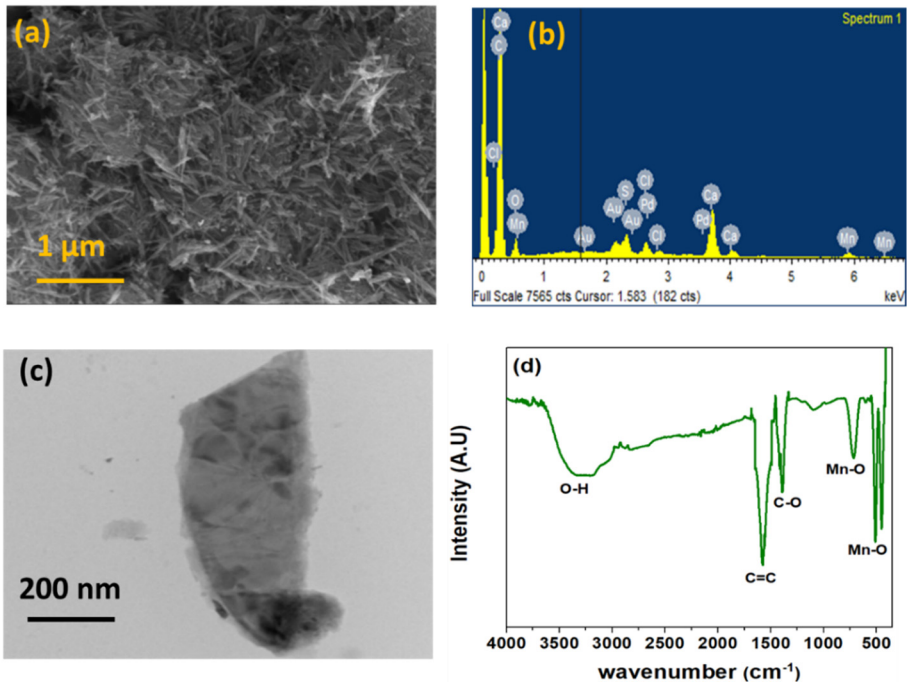

Figure 2. (**a**) SEM micrograph recorded at 20 keV; (**b**) EDX spectrum; (**c**) TEM image obtained at 120 keV; (**d**) FTIR spectrum obtained within 4000–500 cm^{-1} of α-MnO_2/GQD nanocomposites.

3.2. Electrochemical Multiplexed Monitoring of Glucose and Tyrosine

3.2.1. Sensor Stages Response

The fabrication of paper-based multiplexed detection strip was confirmed by performing EIS within 100 Hz–1 MHz, at a sinusoidal amplitude of 100 mV, as shown in Figure 3. The electrolyte chosen for this study was the typical ferrocyanide probe ($[Fe(CN)_6]^{3-/4-}$, 5 mM) prepared in phosphate buffer saline (PBS—0.1 M, pH 6.4) [2].

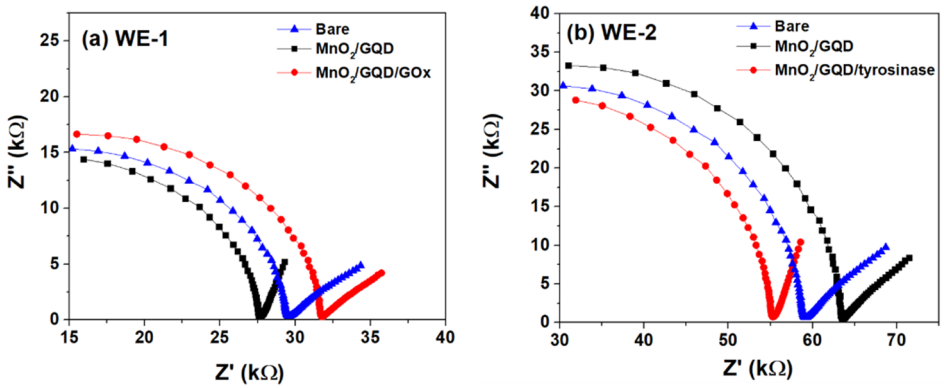

Figure 3. Impedimetric response during various stages of sensor surface modification at (**a**) WE-1; (**b**) WE-2 of the multiplexed strip (WE: working electrode).

The overall sample volume employed in the paper-based sensor is 200 µL. It can be observed that the charge transfer resistance (R_{ct}) increases when WE-2 is connected to the impedance analyzer via a counter electrode. As mentioned in Section 2.5, GOx and tyrosinase enzymes were immobilized on α-MnO_2/GQD-coated working electrodes: WE-1 and WE-2, respectively, with the latter further away from the counter electrode (Figure 1). This situation effectively increases the electron path-length (l), thereby proportionally increasing the path resistance (R α l). Considering the bare (unmodified) electrode, the R_{ct} can therefore be observed to increase from ~30 to ~60 kΩ at WE-1 and WE-2, respectively. Meanwhile in both cases, coating the electrode surfaces with α-MnO_2/GQD nanocomposites decreases

the R_{ct} to ~27.5 kΩ and ~55 kΩ at WE-1 and WE-2, respectively. This is primarily due to the enhanced surface area of the nanocomposites leading to increased heterogeneous electron transfer [32]. However, immobilizing the modified electrode surfaces with GOx and tyrosinase enzymes drastically increases R_{ct} to 32.5 kΩ and ~65 kΩ at WE-1 and WE-2, respectively. Such phenomenon can be attributed to the electrode passivation effect by biomolecules which impede the electron transfer at electrode-electrolyte interface [33]. It must be noted that the occurrence of half semi-circle in Figure 2, in the high frequency region to the left, indicates decreased C_{dl} (or increased Z″, since Z″ α C_{dl}^{-1}) [34,35] due to poor dielectric constant of cellulose paper substrates (C_{dl} α ε). However, the distinct impedance response observed at each step of sensor fabrication indicates the successful development of the multiplexed paper-based diabetes and DFU monitoring strip.

3.2.2. Analytical Performance of Multiplexed Sensor: Benchtop EIS Calibration

The multiplexed monitoring of diabetes and DFUs, as a function of glucose and tyrosine concentrations, were initially assessed with EIS technique within 100 Hz–1 MHz at a small signal amplitude of 100 mV, in PBS-$[Fe(CN)_6]^{3-/4-}$ (0.1 M/5 mM, pH 6.4). The corresponding Nyquist spectra are shown below in Figure 4a,b.

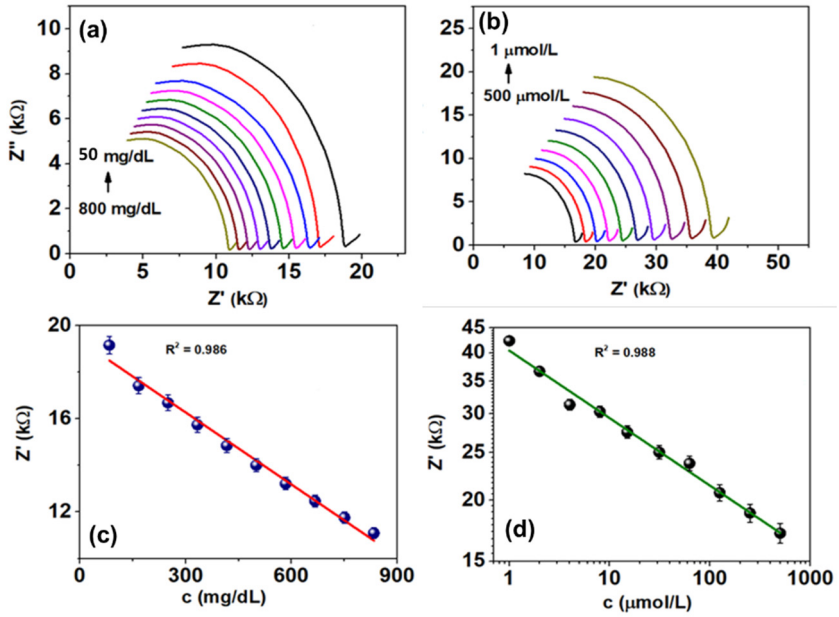

Figure 4. Nyquist spectra obtained from electrocatalytic sensing of (**a**) glucose within 50–800 mg/dL; (**b**) tyrosine within 1–500 µmol/L and sensor calibration at 10 kHz for (**c**) glucose; (**d**) tyrosine monitoring.

Firstly, the occurrence of half-semicircular arcs seems to be preserved as observed in Figure 3, which is primarily due to the poor dielectric constant of the paper substrate. The corresponding Z″ thus increases at lower analyte concentrations, thereby reducing C_{dl}. The latter is also affected by the electrocatalysis of glucose and tyrosine by GOx and tyrosinase respectively. At higher concentrations, the electro-oxidation of glucose to gluconolactone as well as redox cycling between O-quinone and hydroquinone [21,36] (Figure 1) is rapidly enhanced, thereby generating a huge number of electrons which can traverse across the electrode-electrolyte interface. As a result, the R_{ct} at such higher concentrations decreases to ~11.2 kΩ and ~16 kΩ at 800 mg/dL and 500 µmol/L, respectively. The rapid electron transfer essentially charges the electrical double layer, which then leads to high C_{dl} (or low Z″) [2]. Conversely, at lower concentrations, the electrocatalytic electron transfer drastically reduces which results in increased R_{ct}—highlighting poor interface kinetics. This is observed from R_{ct} ~ 18 kΩ and 40 kΩ at 50 mg/dL and 1 µmol/L, respectively. In such a scenario, the double layer charging decreases and hence leads to increased Z″. It can also be observed from Figure 4a,b that R_{ct} for tyrosine detection is comparatively larger

than that for glucose, which is primarily attributed to the inherent geometry of sensing strips as mentioned in Sections 2.5 and 3.2.1.

The developed paper-based microfluidic multiplexed sensor was calibrated at 10 kHz for monitoring both glucose and tyrosine (Figure 4c,d), whereby the electrocatalytic process is unique for each of these analytes. The resulting sensor calibration yields a linear response between Z′ (R_{ct}) and analyte concentration within 50–800 mg/dL (glucose) and 1–500 µmol/L (tyrosine), with goodness-of-fit measures (R^2) of 0.986 and 0.988, respectively. The LoD and sensitivity of the multiplexed sensor towards glucose and tyrosine detection are highlighted in Table 1.

Table 1. Comparison of LoD and sensitivity towards glucose and tyrosine detection using benchtop EIS calibration.

Analyte	LoD	Sensitivity
Glucose	58.30 mg/dL	13.11 kΩ/mg dL^{-1}/mm^2
Tyrosine	0.31 µmol/L	0.71 kΩ/µmol L^{-1}/mm^2

The excellent multiplexed sensing performance obtained using benchtop EIS calibration further motivated us to integrate the developed microfluidic platform with miniaturized electronics.

3.2.3. Implementation of Multiplexed Sensing Strip towards Portable Device Applications

The electrochemical multiplexed monitoring of glucose and tyrosine was performed within 50–800 mg/dL and 1–500 µmol/L, respectively in PBS/$[Fe(CN)_6]^{3-/4-}$ (0.1 M/5 mM, pH 6.4), using a portable resistive device at 5V DC. A similar strategy was adopted in our previous study [37], and is schematically shown in Figure 5.

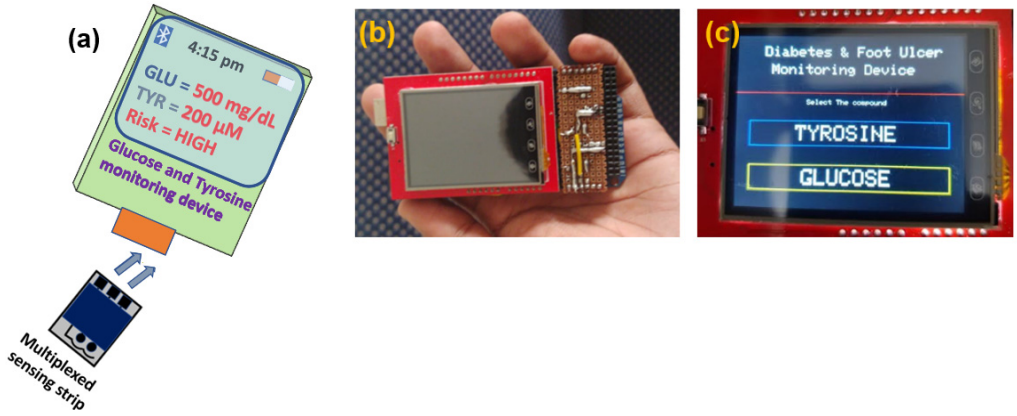

Figure 5. Snapshots of (**a**) integration of multiplexed sensing strip with portable device; (**b**) actual image of portable palm-sized device; (**c**) the display unit of the detection module.

The portable pocket-friendly device is programmed using the Arduino UNO microcontroller board by employing a typical voltage divider network. The latter is primarily used to reduce the supply voltage (5V DC) at the working electrodes (to ~300 mV) to avoid electrolysis and enzyme denaturation. The display unit consists of a touch-screen enabled TFT (thin film transistor) module which highlights the analytes (glucose and tyrosine) to be monitored as a function of sensor resistance. The rationale involves initial indications of diabetes followed by predicting the occurrence of DFUs. However, diabetic patients can directly opt for monitoring tyrosine to avoid the exacerbating consequences of DFUs, thereby having a huge probability of availing timely diagnosis and treatment.

The sensing performance of the portable resistive device towards multiplexed detection of glucose and tyrosine is shown in Figure 6.

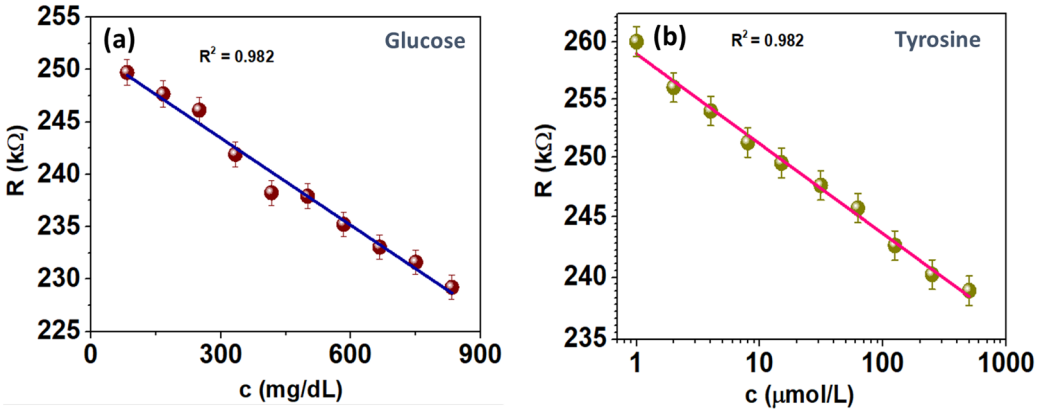

Figure 6. Sensing performance of portable resistive module towards monitoring (**a**) glucose; (**b**) tyrosine at 5V DC supply.

It is interesting to note that the linear nature towards multiplexed sensing of glucose and tyrosine is preserved after interfacing the sensor strip with a portable Arduino UNO-programmed device. The linear range was found to be the same as with benchtop EIS calibration, that is 50–800 mg/dL (glucose) and 1–500 µmol/L (tyrosine), with goodness-of-fit measure (R^2) of 0.982. The LoD and sensitivity of the portable resistive multiplexed sensor towards glucose and tyrosine detection are highlighted in Table 2.

Table 2. Comparison of LoD and sensitivity towards glucose and tyrosine detection using Arduino UNO based portable device.

Analyte	LoD	Sensitivity
Glucose	55.51 mg/dL	0.29 kΩ/mg dL^{-1}/mm^2
Tyrosine	0.87 µmol/L	2.21 kΩ/µmol L^{-1}/mm^2

It is also interesting to observe that the developed Arduino-based portable resistive device generated LoD almost similar to that obtained using the benchtop calibration method, thereby validating the overall multiplexed detection of diabetes and DFU as a function of glucose and tyrosine concentrations, respectively. However, a comparison of the developed portable multiplexed sensor in terms of current status, highlighting its prospects towards PoC monitoring, with respect to few existing ones is shown in Table 3.

Table 3. Comparison of developed portable nanosensor, highlighting its current status with respect to few reported multiplexed platforms.

Sensor Surface	Detection Technique	Remarks	Reference
Silica encapsulated Au nanospheres	SERS	Benchtop calibration, image analysis	[38]
Polydopamine encapsulated Au nanoparticles	SERS	Benchtop calibration, image analysis	[39]
Streptavidin-CdSe/ZnS Quantum dots	ECL	Benchtop calibration, longer wait time/ incubation time	[40]
PAMAM quantum dots	ECL	Benchtop calibration, high applied potential	[41]

Table 3. *Cont.*

Sensor Surface	Detection Technique	Remarks	Reference
Gold nanoparticles	FC	Benchtop calibration, image analysis	[42]
α-MnO_2/GQD	EC	Device-level calibration, faster response, cost-effective tests, scaled till TRL-5	Current Work

Au: gold, CdSe/ZnS: cadmium selenide/zinc sulfide, PAMAM: polyamidoamine, SERS: surface enhanced Raman spectroscopy, ECL: electrochemiluminescence, FC: flow cytometry, EC: electrochemical, TRL: technology readiness level.

3.2.4. Selectivity and Shelf-Life Analysis

The effect of potential interferants on the portable sensor performance is shown in Figure 7a,b. Ascorbic acid (AA) and uric acid (UA) were chosen as the potential interferants since they are common fluid metabolites. The concentration of AA and UA were chosen as 10 µM and 400 µM, respectively. It can be observed that AA and UA generate unique resistance responses, which can be easily distinguished from that of glucose (800 mg/dL) and tyrosine (500 µM) alone. Upon mixing the potential interferants with the target analytes, and spiking them in human serum, it is observed that there is an insignificant deviation in resistance response as seen solely in the case of glucose and tyrosine. Therefore, it can be concluded that the developed Arduino-based multiplexed sensor response does not get affected under the presence of potential metabolites.

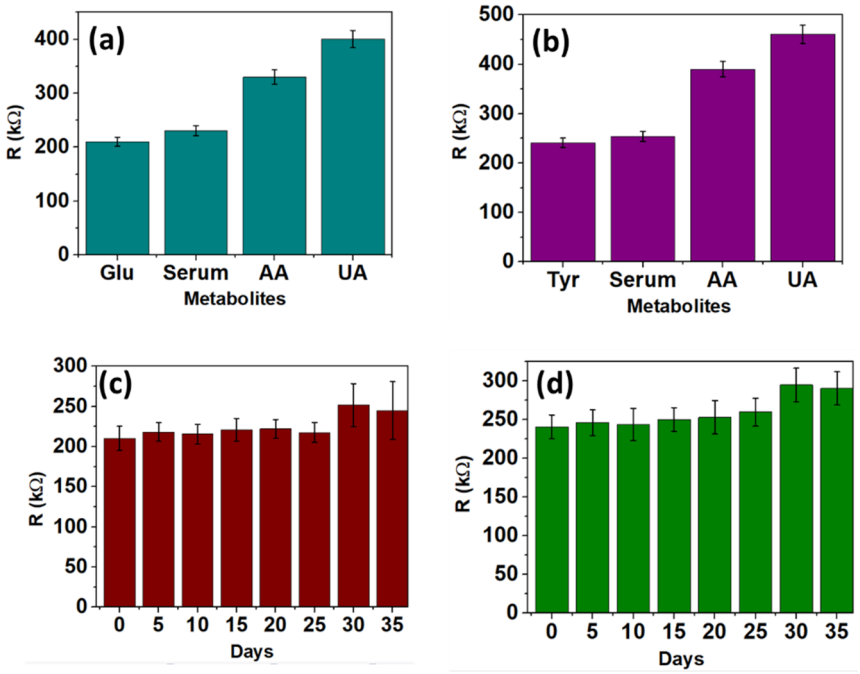

Figure 7. Effect of potential interferants towards the detection of (**a**) glucose; (**b**) tyrosine. The bar "Serum" indicates a mixture of target analytes with interferants spiked in human serum. Shelf-life analysis indicating stability of sensor towards (**c**) glucose; (**d**) tyrosine detection.

Figure 7c,d indicates the stability of the developed portable multiplexed sensing device over a period of 35 days, at intervals of 5 days. It can be observed that the sensor response remains fairly stable up to 25 days, thereby establishing the shelf-life within the specified period, beyond which the sensing strip gets fouled due to enzyme denaturation.

4. Conclusions

An electrochemical microfluidic paper-based sensor for the multiplexed detection of diabetes and diabetic foot ulcer is developed in this study. This essentially works on the enzymatic electrocatalysis of glucose (diabetes) and tyrosine (DFU) resulting in heterogeneous electron transfer, which has been calibrated to specific analyte concentrations. Nanocomposite of α-MnO_2/GQD was coated onto carbon screen-printed working electrodes (diameter ~1 mm), which were further modified by glucose oxidase and tyrosinase enzymes. The benchtop calibration resulted in a linear response within 50–800 mg/dL and 1–500 µmol/L for glucose and tyrosine, with LoDs of ~58 mg/dL and ~0.3 µmol/L, respectively. The platform was further integrated with miniaturized electronics using an Arduino-based microcontroller. The resulting portable resistive sensor accurately detected the presence of glucose and tyrosine at 300 mV DC within the same concentration range, yielding LoDs of 55.51 mg/dL and ~0.87 µmol/L, respectively, which are similar to that observed in the benchtop EIS technique. The sensor response did not get perturbed in the presence of potential interferants, while being stable for 25 days. It can hence be concluded that the portable multiplexed nano-sensor based on a microfluidic platform is highly suitable for early diagnosis of diabetes and eventual prediction of occurrence of DFUs, thereby fitting extremely well within the point-of-care scenario. The future prospect of the developed platform can be extended towards monitoring microbial activity as well in the foot ulcerated site. Specifically, chronic foot ulcers become home for microbial infections, especially by Staphylococcus Aureus (S. Aureus), and as such the complete monitoring of DFUs is of extreme importance. Such a sensing device which can perform multiplexed monitoring of glucose, tyrosine, and S. Aureus can yield a complete package towards diabetes and DFU monitoring, which can eventually be envisaged to be marked development in the biomedical sector for wound monitoring using a point-of-care platform.

Author Contributions: Conceptualization, A.M., S.R. (Shailendra Rajput) and S.W.; methodology, S.R. (Souradeep Roy), S.N. and H.C.N.; validation, S.R. (Souradeep Roy), S.W. and A.M.; formal analysis, S.R. (Souradeep Roy), S.W. and H.C.N.; investigation, S.R. (Souradeep Roy), H.C.N., S.N. and A.M.; resources, A.M. and R.K.; data curation, S.R. (Souradeep Roy), S.N. and R.K.; writing—original draft preparation, S.R. (Souradeep Roy), H.C.N., R.K., S.W. and S.N.; writing—review and editing, S.R. (Shailendra Rajput), S.W. and A.M.; visualization, A.M. and R.K.; supervision, A.M., S.W., R.K. and S.R. (Shailendra Rajput); project administration, A.M.; funding acquisition, A.M. All authors have read and agreed to the published version of the manuscript.

Funding: This research was funded by Department of Science and Technology-UKIERI grant DST/INT/UK/P-131/2016.

Institutional Review Board Statement: Not applicable.

Informed Consent Statement: Not applicable.

Data Availability Statement: The data presented in this study are available on request from the corresponding author.

Acknowledgments: A.M., S.R., S.W. and R.K. would like to acknowledge the flagship project "Smart City" initiated by University of Petroleum and Energy Studies, Dehradun, India. This work is our initial contribution towards this project. The authors would also like to acknowledge Amity University Uttar Pradesh, Noida, India for providing access to experimental facilities.

Conflicts of Interest: The authors declare no conflict of interest.

References

1. Wang, X.; Li, J.; Wang, Z.; Deng, A. Wound exudate CXCL6: A potential biomarker for wound healing of diabetic foot ulcers. *Biomark. Med.* **2019**, *13*, 167–174. [CrossRef] [PubMed]
2. Roy, S.; John, A.; Nagabooshanam, S.; Mishra, A.; Wadhwa, S.; Mathur, A.; Narang, J.; Singh, J.; Dilawar, N.; Davis, J. Self-aligned TiO2—Photo reduced graphene oxide hybrid surface for smart bandage application. *Appl. Surf. Sci.* **2019**, *488*, 261–268. [CrossRef]
3. Kundu, Z.S.; Tanwar, M.; Singh, K.; Singh, B. Clinical Assessment, Risk Factors, and Classification of Diabetic Foot: An Overview. *Clin. Assess.* **2017**, *4*, 35–39. [CrossRef]

4. Sheahan, H.; Canning, K.; Refausse, N.; Kinnear, E.M.; Jorgensen, G.; Walsh, J.R.; Lazzarini, P.A. Differences in the daily activity of patients with diabetic foot ulcers compared to controls in their free-living environments. *Int. Wound J.* **2017**, *14*, 1175–1182. [CrossRef] [PubMed]
5. Maluf, K.S.; Mueller, M.J. Comparison of physical activity and cumulative plantar tissue stress among subjects with and without diabetes mellitus and a history of recurrent plantar ulcers. *Clin. Biomech.* **2003**, *18*, 567–575. [CrossRef]
6. Armstrong, D.G.; Abu-Rumman, P.L.; Nixon, B.P.; Boulton, A.J.M. Continuous activity monitoring in persons at high risk for diabetes-related lower-extremity amputation. *J. Am. Podiatr. Med. Assoc.* **2001**, *91*, 451–455. [CrossRef]
7. Armstrong, D.G.; Lavery, L.A.; Holtz-Neiderer, K.; Mohler, M.J.; Wendel, C.S.; Nixon, B.P.; Boulton, A.J. Variability in activity may precede diabetic foot ulceration. *Diabetes Care* **2004**, *27*, 1980–1984. [CrossRef]
8. Kanade, R.V.; van Deursen, R.W.M.; Harding, K.; Price, P. Walking performance in people with diabetic neuropathy: Benefits and threats. *Diabetology* **2006**, *49*, 1747–1754. [CrossRef]
9. Crews, R.T.; Schneider, K.L.; Yalla, S.V.; Reeves, N.D.; Vileikyte, L. Physiological and psychological challenges of increasing physical activity and exercise in patients at risk of diabetic foot ulcers: A critical review. *Diabetes. Metab. Res. Rev.* **2016**, *32*, 791–804. [CrossRef]
10. Luhar, S.; Kondal, D.; Jones, R.; Anjana, R.M.; Patel, S.A.; Kinra, S.; Clarke, L.; Ali, M.K.; Prabhakaran, D.; Kadir, M.M.; et al. Lifetime risk of diabetes in metropolitan cities in India. *Diabetology* **2020**, *64*, 521–529. [CrossRef]
11. Oyibo, S.O.; Jude, E.B.; Tarawneh, I.; Nguyen, H.C.; Armstrong, D.G.; Harkless, L.B.; Boulton, A.J. The effects of ulcer size and site, patient's age, sex and type and duration of diabetes on the outcome of diabetic foot ulcers. *Diabet. Med.* **2001**, *18*, 133–138. [CrossRef]
12. Nagase, T.; Sanada, H.; Takehara, K.; Oe, M.; Iizaka, S.; Ohashi, Y.; Oba, M.; Kadowaki, T.; Nakagami, G. Variations of plantar thermographic patterns in normal controls and non-ulcer diabetic patients: Novel classification using angiosome concept. *J. Plast. Reconstr. Aesthetic Surg.* **2011**, *64*, 860–866. [CrossRef] [PubMed]
13. Alexovic, M.; Sabo, J.; Longuespee, R. Microproteomic sample preparation. *Protemics* **2021**, *21*, 2000318. [CrossRef]
14. Debats, I.B.; Booi, D.; Deutz, N.E.; Buurman, W.A.; Boeckx, W.D.; van der Hulst, R.R. Infected chronic wounds show different local and systemic arginine conversion compared with acute wounds. *J. Surg. Res.* **2006**, *134*, 205–214. [CrossRef]
15. Felitsyn, N.M.; Henderson, G.N.; James, M.O.; Stacpoole, P.W. Liquid chromatography-tandem mass spectrometry method for the simultaneous determination of δ-ALA, tyrosine and creatinine in biological fluids. *Clin. Chim. Acta* **2004**, *350*, 219–230. [CrossRef]
16. Ishii, Y.; Iijima, M.; Umemura, T.; Nishikawa, A.; Iwasaki, Y.; Ito, R.; Saito, K.; Hirose, M.; Nakazawa, H. Determination of nitrotyrosine and tyrosine by high-performance liquid chromatography with tandem mass spectrometry and immunohistochemical analysis in livers of mice administered acetaminophen. *J. Pharm. Biomed. Anal.* **2006**, *41*, 1325–1331. [CrossRef] [PubMed]
17. Latorre, R.M.; Saurina, J.; Hernández-Cassou, S. Determination of amino acids in overlapped capillary electrophoresis peaks by means of partial least-squares regression. *J. Chromatogr. A* **2000**, *871*, 331–340. [CrossRef]
18. Roy, A.K.; Nisha, V.S.; Dhand, C.; Malhotra, B.D. Molecularly imprinted polyaniline film for ascorbic acid detection. *J. Mol. Recognit.* **2011**, *24*, 700–706. [CrossRef] [PubMed]
19. Kong, F.Y.; Li, X.R.; Zhao, W.W.; Xu, J.J.; Chen, H.Y. Graphene oxide–thionine–Au nanostructure composites: Preparation and applications in non-enzymatic glucose sensing. *Electrochem. Commun.* **2012**, *14*, 59–62. [CrossRef]
20. Singhal, C.; Dubey, A.; Mathur, A.; Pundir, C.S.; Narang, J. Paper based DNA biosensor for detection of chikungunya virus using gold shells coated magnetic nanocubes. *Process Biochem.* **2018**, *74*, 35–42. [CrossRef]
21. Apetrei, I.M.; Apetrei, C. Development of a Novel Biosensor Based on Tyrosinase/Platinum Nanoparticles/Chitosan/Graphene Nanostructured Layer with Applicability in Bioanalysis. *Materials* **2019**, *12*, 1009. [CrossRef]
22. Yang, X.; Cheng, H. Recent Developments of Flexible and Stretchable Electrochemical Biosensors. *Micromachines* **2020**, *11*, 243. [CrossRef] [PubMed]
23. Economou, A.; Kokkinos, C.; Prodromidis, M. Flexible plastic, paper and textile lab-on-a chip platforms for electrochemical biosensing. *Lab Chip* **2018**, *13*, 1812–1830. [CrossRef] [PubMed]
24. Jia, H.; Cai, Y.; Lin, J.; Liang, H.; Qi, J.; Cao, J.; Feng, J.; Fei, W. Heterostructural Graphene Quantum Dot/MnO2 Nanosheets toward High-Potential Window Electrodes for High-Performance Supercapacitors. *Adv. Sci.* **2018**, *5*, 1700887. [CrossRef] [PubMed]
25. Yan, X.; Song, Y.; Zhu, C.; Song, J.; Du, D.; Su, X.; Lin, Y. Graphene Quantum Dot-MnO2 Nanosheet-Based Optical Sensing Platform: A Sensitive Fluorescence "Turn Off-On" Nanosensor for Glutathione Detection and Intracellular Imaging. *Appl. Mater. Interfaces* **2016**, *8*, 21990–21996. [CrossRef]
26. Dong, Y.; Shao, J.; Chen, C.; Li, H.; Wang, R.; Chi, Y.; Lin, X.; Chen, G. Blue luminescent graphene quantum dots and graphene oxide prepared by tuning the carbonization degree of citric acid. *Carbon* **2012**, *50*, 4738–4743. [CrossRef]
27. Dubey, M.; Challagulla, N.V.; Wadhwa, S.; Kumar, R. Ultrasound assisted synthesis of magnetic Fe3O4/α-MnO2 nanocomposite for photodegradation of organic dye. *Colloids Surf. A Physicochem. Eng. Asp.* **2021**, *609*, 125720. [CrossRef]
28. Kumar, R.; Sithambaram, S.; Suib, S.L. Cyclohexane oxidation catalyzed by manganese oxide octahedral molecular sieves-Effect of acidity of the catalyst. *J. Catal.* **2009**, *262*, 304–313. [CrossRef]
29. Roy, S.; Nagabooshanam, S.; Wadhwa, S.; Kumar, R.; Mathur, A.; Dubey, A.K. A label-free impedimetric sensor based on αmnO2/tyrosinase hybrid for monitoring of diabetic foot ulcers. In Proceedings of the 2020 7th International Conference on Signal Processing and Integrated Networks (SPIN), Noida, India, 27–28 February 2020; pp. 1157–1161. [CrossRef]

30. Wang, H.; Lu, Z.; Qian, D.; Li, Y.; Zhang, W. Single-crystal α-MnO2 nanorods: Synthesis and electrochemical properties. *Nanotechnology* **2007**, *18*, 115616. [CrossRef]
31. Choudhary, R.P.; Shukla, S.; Vaibhav, K.; Pawar, P.B.; Saxena, S. Optical properties of few layered graphene quantum dots. *Mater. Res. Express* **2015**, *2*, 095024. [CrossRef]
32. Rana, A.; Killa, M.; Yadav, N.; Mishra, A.; Mathur, A.; Kumar, A.; Khanuja, M.; Narang, J.; Pilloton, R. Graphitic Carbon Nitride as an Amplification Platform on an Electrochemical Paper-Based Device for the Detection of Norovirus-Specific DNA. *Sensors* **2020**, *20*, 2070. [CrossRef] [PubMed]
33. Bai, Y.H.; Zhang, H.; Xu, J.J.; Chen, H.Y. Relationship between nanostructure and electrochemical/biosensing properties of MnO2 nanomaterials for H2O 2/choline. *J. Phys. Chem. C* **2008**, *112*, 18984–18990. [CrossRef]
34. Lvovich, V.F. Fundamentals of Electrochemical Impedance Spectroscopy. *Impedance Spectrosc.* **2012**, 1–21. [CrossRef]
35. Katz, E.; Willner, I. Probing biomolecular interactions at conductive and semiconductive surfaces by impedance spectroscopy: Routes to impedimetric immunosensors, DNA-sensors, and enzyme biosensors. *Electroanalysis* **2003**, *15*, 913–947. [CrossRef]
36. Rakhi, R.B.; Nayak, P.; Xia, C.; Alshareef, H.N. Novel amperometric glucose biosensor based on MXene nanocomposite. *Sci. Rep.* **2016**, *6*, 36422. [CrossRef] [PubMed]
37. Gupta, A.K.; Khanna, M.; Roy, S.; Pankaj; Nagabooshanam, S.; Kumar, R.; Wadhwa, S.; Mathur, A. Design and development of a portable resistive sensor based on α-MnO2/GQD nanocomposites for trace quantification of Pb(II) in water. *IET Nanobiotechnol.* **2021**, *15*, 505–511. [CrossRef]
38. Lee, S.; Chon, H.; Lee, J.; Ko, J.; Chung, B.H.; Lim, D.W.; Choo, J. Rapid and sensitive phenotypic marker detection on breast cancer cells using surface-enhanced Raman scattering (SERS) imaging. *Biosens. Bioelectron.* **2014**, *51*, 238–243. [CrossRef]
39. Sun, C.; Zhang, L.; Zhang, R.; Gao, M.; Zhang, X. Facilely synthesized polydopamine encapsulated surface-enhanced Raman scattering (SERS) probes for multiplex tumor associated cell surface antigen detection using SERS imaging. *RSC Adv.* **2015**, *5*, 72369–72372. [CrossRef]
40. Guo, Z.; Hao, T.; Du, S.; Chen, B.; Wang, Z.; Li, X.; Wang, S. Multiplex electrochemiluminescence immunoassay of two tumor markers using multicolor quantum dots as labels and graphene asconductingbridge. *Biosens. Bioelectron.* **2013**, *44*, 101–107. [CrossRef]
41. Babamiri, B.; Hallaj, R.; Salimi, A. Ultrasensitive electrochemiluminescence immunoassay for simultaneous determination of CA125 and CA15-3 tumor markers based on PAMAM-sulfanilic acid-Ru(bpy)32+ and PAMAM-CdTe@CdS nanocomposite. *Biosens. Bioelectron.* **2018**, *99*, 353–360. [CrossRef]
42. Jiang, Y.; Tang, Y.; Miao, P. Polydopamine nanosphere@silver nanoclusters for fluorescence detection of multiplex tumor markers. *Nanoscale* **2019**, *11*, 8119–8123. [CrossRef] [PubMed]